Biochimica et Biophysica Acta, 1100 (1992) 15–26

BBABIO 43582

The flash-induced turnover of cytochrome *b*-563, cytochrome *f* and plastocyanin in chloroplasts. Models and estimation of kinetic parameters

A.B. Hope [a], R.R. Huilgol [b], M. Panizza [b], M. Thompson [c] and D.B. Matthews [c]

Schools of [a] Biological Sciences, [b] Information Science and Technology and [c] Physical Sciences, Flinders University, Adelaide (Australia)

(Received 21 November 1991)

Key words: Photosynthesis; Electron transfer; Cytochrome *b/f* complex; Model; Inverse Method; Plastocyanin; (Pea)

Flash-induced redox changes of cytochrome *b*-563, cytochrome *f* and plastocyanin (PC), and the electrochromic response from chloroplast suspensions in reducing conditions (added dichlorophenyldimethylurea, exogenous quinol, anaerobic) were measured in the time range 0–20 ms by deconvoluting absorbance changes at appropriate wavelengths. No response attributable to cytochrome *b*-559 was observed. Various dimethylbenzoquinols with different substituents on the 6-position of the benzene ring gave similar kinetics for these processes. There was no significant effect on cytochrome *b*-563, *f* or PC kinetics of adding nonactin to decay the transthylakoid electric potential difference. These data, together with comparable data for proton deposition, were used in a parameter optimisation procedure, the Inverse Method, to produce rate coefficients for some of the partial reactions occurring when cytochrome *f* is oxidised by plastocyanin and quinol is subsequently oxidised by cytochrome *b/f* complexes. Models such as the Q-cycle or semiquinone (SQ) cycle were used to formulate differential equations describing the time-dependencies of various forms of the cytochrome *b/f* complex containing reduced or oxidised cytochrome *f*, Rieske centre, cytochrome *b*-563, and so forth. The Inverse Method minimised the error between data and corresponding model predictions by adjusting parameter values. A model with the two *b*-563 cytochromes not directly connected electronically was unsatisfactory; Q-cycle and SQ-cycle models could not be differentiated by the available data. A Q-cycle model gave a close match in all respects between data and model predictions using 8 rate coefficients. The following average, reduced rate-coefficients (s^{-1}) were estimated for the chloroplast cytochrome *b/f* complex under the conditions used: k_{FP} (between cytochrome *f* and PC) 2000; k_{PF} (reverse) 220; k_{QR} (between quinol and Rieske centre) 200; k_{HQ} (between cytochrome *b*-563 (high potential) and quinone at n-sites) 380; k_{QH} (reverse) 150. The Rieske centre and cytochrome *f* appeared to be in rapid equilibrium, with an equilibrium constant of about 3, Rieske positive to *f*.

Introduction

To understand the operation of the cytochrome *b/f* complex in chloroplasts, details are needed of the reactions involving plastoquinone, plastoquinol, the Rieske centre, cytochrome *f*, plastocyanin and the two *b*-cytochromes, *b*-563 (low potential) and *b*-563 (high potential). These reactions take place in or near at least four locations on the *b/f* complex: the so-called p- and n-sites (Q_o and Q_r sites), near the Rieske centre and near the cytochrome *f* subunit.

In addition, there are indications of another site, producing the 'G' signal [1], which, however, is said to be absent from chloroplasts. Another possible compo-

Abbreviations: cytochrome *b*-563(L,H), with low or high standard reduction potential; DCMU, 3-(3,4-dichlorophenyl)1,1-dimethylurea; DQH_2, duroquinol; EC, electrochromic shift (in absorption spectrum due to an electric field); E_m, standard reduction potential; $FeS(^+)$ or R, Rieske iron/sulphur centre (oxidised); Hepes, *N*-2-hydroxyethylpiperazine-*N*-2-ethanesulphonic acid; k_{FP}, k_{RF}, etc., reduced rate-coefficients as defined in the text; n-site, site assumed to bind PQ in a *b/f* complex near the stroma side of the thylakoid membrane; $PC(^+)$, plastocyanin (oxidised); PMS, phenazine methosulphate; PMT, photomultiplier tube; $PQ(H_2)$, plastoquinone (-ol); $PQH(^+)$, plastosemiquinone (cation); PQH_2^{2+}, plastoquinone di-cation; PQ^-, plastoquinone radical anion; PQ^{2-}, plastoquinone dianion; PS I, PS II, Photosystem I, II; Pr-BQH_2, 6-propyl, 2, 3-dimethylbenzoquinol; $P700(^+)$, reaction centre (oxidised) in PS I; p-site, site assumed to bind PQH_2 on a *b/f* complex near the inside of a thylakoid; SQ, semi-quinone; *(F)RH*, *(F)R⁺H*, *(F)Rp⁺H*, *(F)RH⁻n*, *(F)RHn⁻*, *(F)R⁺H⁻n*, *(F)R⁺Hn⁻*, *(F)Rp⁺H⁻n*, forms of the cytochrome *b/f* complex in states of oxidation or reduction explained in Appendix 1; ΔH_n^+, ΔH_p^+, extent of proton uptake at n-sites, or deposition at p-sites.

Correspondence: A.B. Hope, School of Biological Sciences, Flinders University, GPO Box 2100, Adelaide, SA 5001, Australia.

nent associated with the b/f complex is low-potential cytochrome b-559; though detected in redox titrations of isolated b/f complexes [2], we shall conclude (Discussion) that it does not turn over in flashes given in reducing conditions.

Various data exist for some of the reactions associated with the cytochrome b/f complex, in a large variety of conditions, and in intact cells [3,4], heterocysts [5], isolated thylakoids [6–9], reconstituted systems in solution [10] or in vesicles [11], and isolated b/f complexes [12,13]. Because available data are scattered and not easily comparable, and with chloroplasts do not show satisfactory detail of the kinetics of each of cytochrome b-563, f and PC turnover, our aim has been to measure as many as practicable of the electron and proton transfer reactions with standardised chloroplast preparations, and to develop a quantitative kinetic description of light-induced electron transfer between the two photosystems. Some results have already been reported [14,15].

The Rieske centre has a meagre optical spectral response between the oxidised and reduced states [16,17] and its kinetics following a flash have not yet been observed. However, the response of cytochrome f can be used in models to make inferences about that of the Rieske centre (Discussion).

The two b-563 cytochromes have reduced-minus-oxidised spectra with the same [18], or narrowly separated [12] peak wavelengths. Despite this closeness of properties, from experimental findings and theoretical considerations it is clear that the component returning a redox signal under most conditions is cytochrome b-563 (high potential). The arguments are presented later.

Data have been obtained that lead to the average, flash-induced, deconvoluted redox responses of cytochrome f, cytochrome b-563, PC and the slow electrochromic (EC) bandshift signal at 520 nm, both in the presence and absence of the field-reducing ionophore nonactin. The signal-to-noise ratio was appropriate to show detailed kinetics in the time range 0.1 to 20 ms after a single-turnover laser flash. The 'Inverse Method' was used to produce kinetic parameters that were optimal with respect to the differences between data points and corresponding model predictions. As well as the new data for cytochrome b-563, cytochrome f, PC and the slow EC signal, new and comparable data for proton deposition were also used in this procedure. This approach extends and refines earlier modelling attempts [15].

Material and Methods

Pea chloroplasts were prepared as previously described [14]. Thylakoid suspensions were made by osmotic shock: injecting concentrated chloroplasts into 5 ml of dilute buffer made of (mM) 10 KCl, 3 $MgCl_2$, 10 Hepes/KOH (pH 7.8), followed by the addition of 5 ml of 660 sorbitol, 10 KCl, 3 $MgCl_2$, 10 Hepes/KOH (pH 7.8), such that the final [Chl] was 20 μM. These solutions had been initially bubbled with N_2. The final suspension also contained 10 μg/ml of glucose oxidase, 10 μM DCMU, 400 μM duroquinol (or other quinols and concentrations as specified) and 5 mM glucose. After mixing, there was no further stirring.

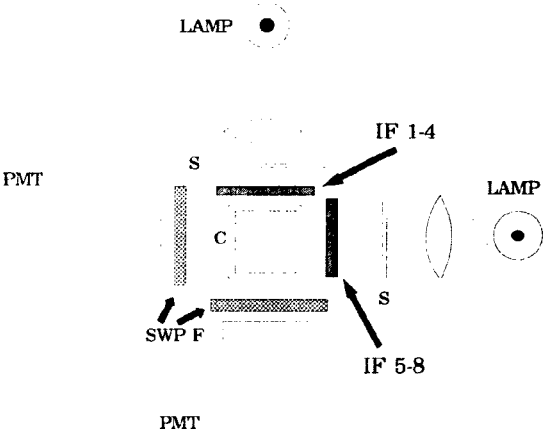

Fig. 1. Experimental set-up used to measure flash-induced absorbance changes at up to 8 wavelengths, in a suspension of thylakoids: C, cuvette with 18 mm pathlength and containing 10 ml of suspension (composition in Methods); S, Uniblitz 25 mm diam. electronic shutters; IF, interference filters, in sets of four, mounted on a stepper motor-driven wheel which rotated 90° after each flash; SWPF, short-wave pass Corning blue-green filters; PMT, Thorn-EMI type 9658B photomultiplier tubes with 8 dynodes in use; light-emitting diodes (LED's) provided steady light equal to that of the measuring beams to the photocathodes while the measuring beams were shuttered off; the LED's were extinguished in synchrony with the shutter opening; laser flashes were reflected downward into the cuvette with a 45° mirror.

Experiments were done in an eight-wavelength spectrophotometer outlined in Fig. 1. Each of the two measuring beams, of four possible wavelengths selected sequentially by the interference filter carriers, was shuttered on for only a short time (c. 100 ms) before data collection started, to minimise turnovers not due to the flash. The interference filters (Omega Optical, USA) were of 1 nm bandwidth. The flash, of duration 15 ns and energy at the cuvette of up to 10 mJ, was from a YAG laser with Q-switching, modified for frequency-doubling to 532 nm, and Raman shifting to 685 nm with a high-pressure hydrogen tube; near the cuvette, which had a reflecting base, the laser beam was expanded to above 10 mm. We used a larger than usual cuvette to enhance the signal-to-noise ratio.

With 10 mJ flash energy, about 80 photons were incident per chloroplast reaction centre. Halving this energy did not alter the results, so the flash was saturating. The PMT's were partly protected from laser light with BG-18 (Corning) sh. t-wave pass filters. The flash produced an artifact which obscured the chloroplast kinetics for about 50 μs.

Data from a two-channel, analogue amplifier with response time-constant of about 10 μs went to a two-channel analogue-to-digital converter; integer numbers from the latter were accumulated in wavelength-related arrays for a number of flashes at usually 0.2 Hz. Deconvolution of the data at wavelengths 520, 554, 564 and 575 nm to produce the separate contributions due

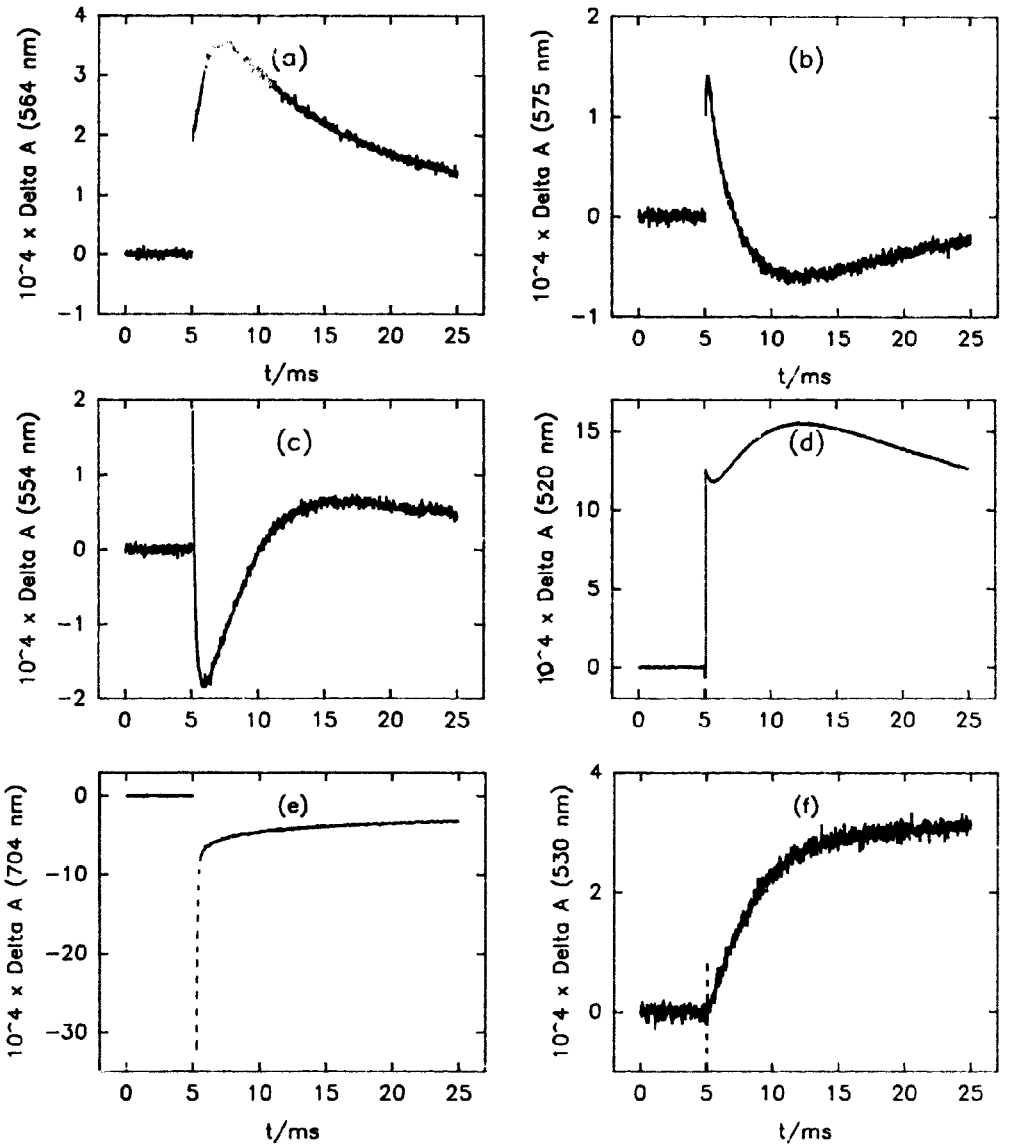

Fig. 2. Primary data for the absorbance changes vs. time in ms, at the wavelengths (a) 564, (b) 575, (c) 554, (d) 520, (e) 704 nm; the dashed portion of the last is the assumed time-course (obscured by strong fluorescence) starting from ~32 units (fully oxidised P700), the composition of the suspension medium is given in Material and Methods. (f) is the neutral red-dependent signal at 530 nm, i.e. (+ NR)-(- NR), representing proton deposition; [NR] was 20 μM, external buffering was from 5 mM Hepes/KOH (pH 7.5). The signals are averages of several experiments with fresh suspensions, each set being repeated with several chloroplast preparations; up to 1300 flashes were given at each wavelength. The A/D converter was programmed to perform 1000 samplings at 25 μs intervals with usually 128 repeats at 0.2 Hz, the laser flash occurring at 5 ms on the time axis.

to the electrochromic shift at 520, cytochrome *f* at 554, cytochrome *b*-563 at 564 and PC at 575 nm was done by a method similar to that of Rich et al. [10] with a 4 × 4 matrix, after subtraction of (small) spectral changes at these wavelengths due to P700. This was done using data obtained at 700 nm, where other components contributed negligible absorbance changes. Data from the wavelength 559 nm was included in a 5 × 5 matrix to check for a possible signal due to cytochrome *b*-559. If methyl viologen were used as an electron acceptor for PS I, as in Refs. 14 15, significant absorbance changes at 520–575 nm, due to its flash-induced reduction, were difficult to deconvolute. Methyl viologen was therefore omitted from the suspension medium. That PS I turnovers were not diminished was shown by the equal size of the fast and slow EC signals with or without added acceptor; presumeably traces of oxygen were sufficient to accept electrons.

Reference spectra for the redox changes in absorbance of cytochrome *f*, cytochrome *b*-563, PC, P700 and the EC shift were kindly provided by P.R. Rich (personal communication); further spectra were obtained from purified PC and *b*/*f* complexes in the laboratory of G. Hauska. The relative contributions of

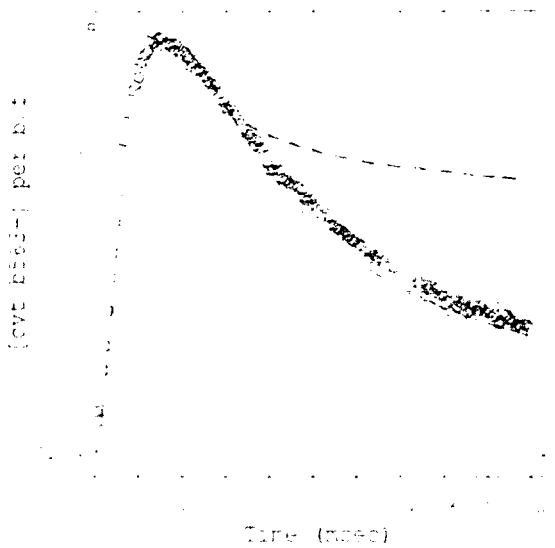

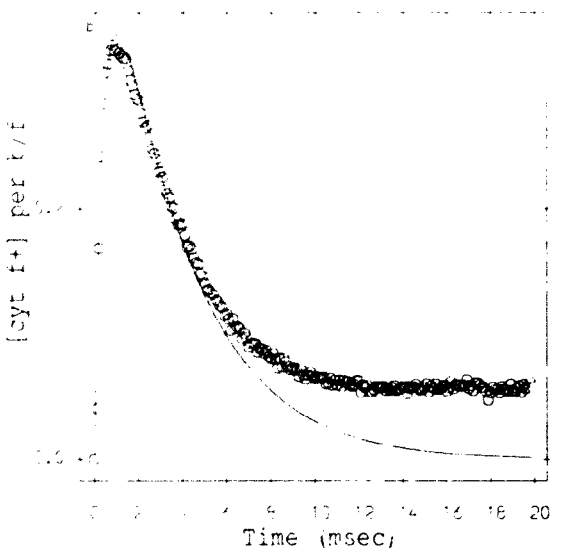

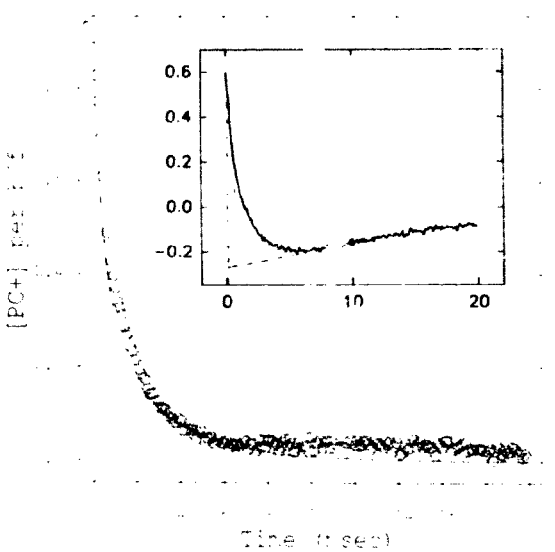

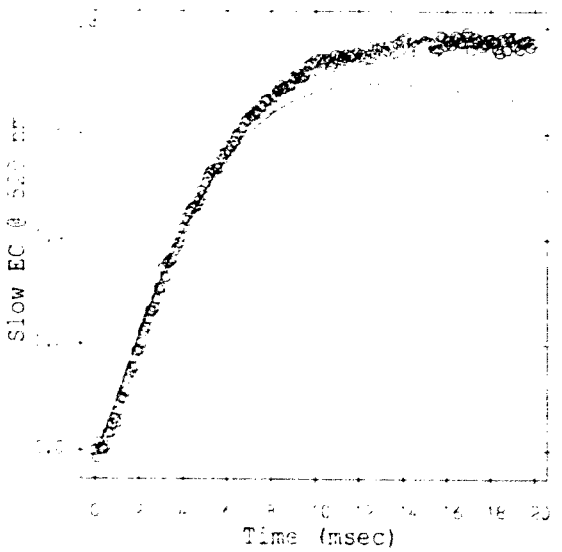

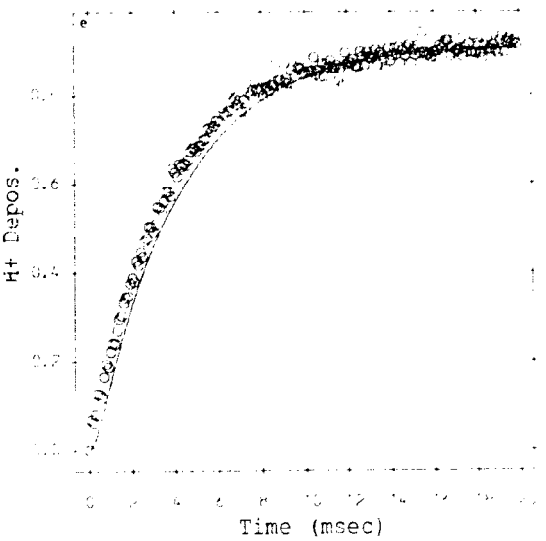

Fig. 3. (continued).

the electrochromic shift at the above wavelengths were also estimated from literature data [19,20] and our own measurements of the relative nonactin-dependent signal at 1–2 ms after a flash. Together, these figures were used to construct the relevant matrix. The relative extinction coefficients adopted for the 4×4 matrix are given in Table I. The values adopted for the relative and absolute extinction coefficients do not differ significantly from those used by Rich et al. [10] nor, except for cytochrome *b*-563, from those tabulated by de Wolf et al. [11].

2,3-Dimethyl-6-alkyl-1,4-benzohydroquinones were synthesised by a Fries rearrangement of 2,3-dimethylphenyl esters followed by reduction of the carbonyl group and oxidation by dichromate to the 1,4-benzoquinone. Reduction gave stable trialkylquinols. They were dissolved in acidic DMSO to make stock solutions of 200–250 mM.

TABLE I

Relative extinction coefficients for the deconvoluted components at the measuring wavelengths

In calculating the extent of oxidation or reduction, the following extinction coefficients (mM^{-1} cm^{-1}) were used: for cytochrome *b*-563(H) at 564 nm, 16.2 [12]; cytochrome *f* at 554 nm, 18 [10,12]; PC at 575 nm, 4.16 [10]; P700 at 704 nm, 60 (calculated from the value 64 at 700 nm)

Wavelength / nm	Component			
	cyt *b*-563	cyt *f*	PC	EC
520	−0.038	0.068	0.258	1.000
554	0.165	1.000	0.668	0.073
564	1.000	−0.210	0.827	0.070
575	−0.135	−0.230	1.000	−0.010

Results

(a) The deconvolution of the separate components

Fig. 2 shows the primary data used in deconvolutions, (a–e), or directly in modelling (proton deposition, f). The data are averages of signals from several chloroplast suspensions from each of several preparations on different days. Fig. 3 (i.e., the circles; the fitted curves are discussed below) shows the deconvoluted data representing the flash-induced responses of cytochrome *b*-563, cytochrome *f* and PC, together with the slow EC signal. This last was obtained from the difference in deconvoluted EC signals without and with 2 μM stigmatellin. Addition of 2 μM nonactin caused only minor differences in the kinetics of cytochrome *b*-563, cytochrome *f* or PC. Compared with earlier published traces and data for cytochrome *b*-563 kinet-

Fig. 3. Deconvoluted data (circles) representing flash-induced redox changes in (a) cytochrome *b*-563 (reduction upwards), (b) cytochrome *f* (oxidation upwards) and (c, inset) PC (oxidation upwards); (d) is the time-course of the slow electrochromic signal and (e) that of proton deposition, obtained with procedures described in the text or the Fig. 2. legend. The *y*-axes in (a)–(c) have the units of mol/mol *b*/*f* complex, the *x*-axes have units of ms. The slow phase of the EC signal was scaled to a fast phase of 1.0, while the proton deposition was normalised to the same maximum as given by the model: 0.9 means 1.8 H^+ deposited per cytochrome *b*/*f*. The data in the shaded area of the inset to (c) are the circles in the main diagram, and were used in modelling. Only the first 7 ms of data were used in Inverse Method parameter optimisation, to achieve convergence of the solution otherwise skewed by the increasing divergences in the 7–20 ms range, especially in the cytochrome *f* data. However, the solution was extended to 20 ms as plotted. The full lines are the predicted time-courses obtained from model Q-cycle 2 using the optimised rate-coefficients: k_{FP}, 1880; k_{PF}, 248, k_{RF}, $7.3 \cdot 10^4$; k_{FR}, $2.4 \cdot 10^5$; k_{QH}, 125; k_{HQ}, 349; k_{QR}, 305; k_D 56 s^{-1}. The dashed line for cytochrome *b*-563 is for a fixed k_D of 5 s^{-1} (see Discussion). The data used were derived from those in Fig. 2 with some smoothing (1 value from 3 points separated by 25 μs, averaged at each 100 μs: $y = (y_{n-1} + y_n + y_{n+1})/3$) to give a more manageable 200 data points. The simulated EC signal was calculated (cf. Ref. 24) from solutions for the time-variations in species representing charge separated across the thylakoids:

$$EC(520) = \exp(-35t) \cdot \{\Delta H_n^+ + ([FRH^+ n] + [F^- RH^+ n] + [FK^+ H^+ n])/2 + [FRHn^+] + [F^- RHn^+] + [FR^- Hn^+]\}$$

where the first term represents a decay with a rate coefficient set equal to that observed for the fast phase (+ stigmatellin), the second, the fully delocalised charge associated with OH-left on the n-side after proton uptake, the third group represents electrons on cytochrome *b*-563(H) halfway across the membrane and the last group, electrons on species with a radical PQ bound to n-sites. It is clear that the slow EC phase decays slower than the fast phase (+ stigmatellin).

ics (see, for example, Refs. 6,15), its reduction was faster ($t_{1/2} < 1$ ms, compared with 1.5–3 ms). This is due to more careful preparation of stable DQH_2 solutions, and to the proper allowance being made for the EC contribution and the PC signal; in the past the PC contribution at 575 nm has been wrongly included in the subtraction $\Delta A_{563}-\Delta A_{575}$ used to calculate Δ[cytochrome *b*-563].

The deconvolution produced negative values for $[PC^+]$ at times greater than approx. 2 ms, followed by a slowly-rising portion (inset, Fig. 3c). The latter trend was clearly due to its slow reduction of $P700^+$ (Fig. 2e). Thus, between flashes, some PC was in the oxidised state. However, the general shape is that expected of PC: rapid oxidation (not resolved) and re-reduction by cytochrome *f* which has a complex time-course because some *b/f* complexes have double turnovers. These aspects are closely matched by the models discussed below, when the changes in $[PC^+]$ in the shaded area of Fig. 3 (c, inset) are taken as the relevant data.

A check that the behaviour of the cytochromes was being reasonably deconvoluted was provided by experiments (not shown) in the presence of stigmatellin, which prevents the reduction of oxidised cytochrome *f* or Rieske centre in the cytochrome *b/f* complex. The expected results were observed, namely absence of reduced cytochrome *b*-563 and almost no re-reduction of oxidised cytochrome *f*.

Because the reduction kinetics for cytochrome *b*-653 now appeared faster, we repeated the experiments reported earlier [15] on the effect of quinol concentration; the rate-coefficients generally increased with $[Pr\text{-}BQH_2]$ as found before with DQH_2, but all the rates were correspondingly greater (not shown). The differences were not due to a different quinol being used (see (b) below). The rate-coefficients for re-reduction

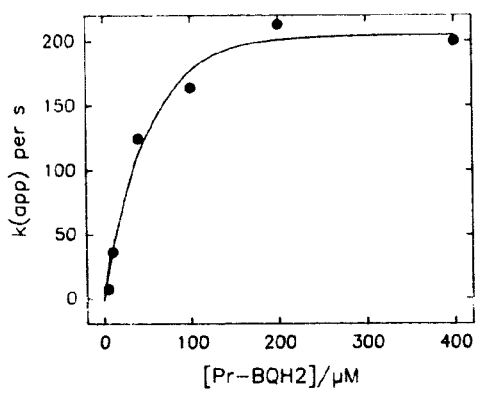

Fig. 4. Rate-coefficient, k_{app}, for the re-reduction of oxidised cytochrome *f*, as a function of the concentration of propyl benzoquinol. This coefficient was estimated from the time to return from the peak to half-peak values. Conditions were approximately as for Fig. 2, except that the degree of anaerobiosis was not so complete.

TABLE II

Models used in conjunction with the inverse method for data fitting

Model Name	No. Eqns.	No. fittable parameters	Distinguishing features
Q-cycle 1	15	8	Fast e transfer between haems $[f^+]$ calc as fraction of holes (fast $f \leftrightarrow$ R equilibrium)
SQ-cycle 1	15	8	as above plus PQ^- can reduce *b*(H) directly
Q-cycle 2	15	8	$k_{QL} \gg$ other *k* values $f \leftrightarrow$ R equilibrium explicit
SQ-cycle 2	17	8	as Q-cycle 2 plus PQ^- can reduce *b*(H) directly
Q-cycle 3	11	7	$k_{QL} \gg$ other *k* values otherwise as Q-cycle 1
SQ-cycle 3	14	9	as SQ-cycle 1 but no direct *b*(L):*b*(H) interaction

of flash-oxidised cytochrome *f* are shown as a function of $[Pr\text{-}BQH_2]$ in Fig. 4. The maximum extent of oxidation did not appear to depend on [quinol].

(b) The effect of different quinols

6-Propyl-, -decyl- and -heptadecyl-2,3-dimethylbenzoquinol behaved similarly to duroquinol (tetramethylbenzoquinol). 2,3-Dimethylbenzoquinol promoted little flash-induced cytochrome turnover compared with the other quinols. Though the possibility cannot be excluded that the several quinols each acted directly as the reductant for oxidised *b/f* complexes, the similar rate-coefficients for the four effective quinols suggest that they acted as mediators in reducing the pool of PQ, and that PQH_2 was the immediate electron donor to *b/f* complexes as concluded previously [14]. Using much greater flash rates, Rich et al. [21] showed that DQH_2 became the reductant for *b/f* complexes.

(c) Modelling, and the Inverse Method

Two generic models were considered: the Q-cycle [22] and the semiquinone (SQ) cycle [23]. Preliminary modelling of the Q-cycle has already been attempted: a step-wise model, without kinetic characterisation [24], and a kinetic model [15]. One of the present models (Q-cycle 1) is similar to the latter; a second (Q-cycle 2) included cytochrome *f* as well as the Rieske centre. Several SQ-cycle models were tried, with the common property that the species PQ^- could traverse the membrane and reduce either of *b*-563(L) or (H). In models SQ-cycle 1 and 2, the haems were in addition connected electronically with fast, irreversible transfer from L to H. In model SQ-cycle 3 the haems were unconnected within their subunit (cf. [25]). Features of these models are summarised in Table II.

TABLE III

Optimised parameters from the inverse method

The parameters are reduced rate-coefficients; that is, they are referred to unit concentration in each case and have the units s^{-1}. The quantity Δ is related to the sensitivity of the integral error to changes in the parameter. Its sign is not relevant to the conclusions, but a small value relative to the parameter value indicates a firmly-established result. The quantity $I[\mathbf{p}]$ is the integral error as defined in Appendix 2. Generally, the differential equations were seeded with parameters likely to enable the solution to reach a global minimum error. α is the fraction of holes (electron deficits) that are in cytochrome *f*, the remainder being assumed to be on R, the Rieske centre. α was optimised by seeding with a likely value and finally varying its size to find the minimum error, keeping the other parameters fixed, with a repetition of the process if necessary

Parameter (s^{-1})	Q-cycle 1 (Δ)	Q-cycle 2 (Δ)	SQ-cycle 3 (Δ)
k_{RP}	2250 (48)	–	2074 (−9)
k_{PR}	209 (10)	–	565 (23)
k_{QR}	74 (0.3)	305 (−4.6)	40 (−0.1)
k_{QL}	26500 (−17000)	–	8800 (2500)
k_{LQ}	–	–	200 (−12)
k_{HQ}	407 (−3.2)	350 (0.7)	$1.3\cdot10^{6}$ (6300)
k_{QH}	170 (−32)	125 (−1.3)	$2.8\cdot10^{5}$ ($-4\cdot10^{4}$)
k_{D}	96 (−2.4)	56 (−1.7)	260 (11)
α	0.73	–	0.70
k_{FP}	–	1880 (13)	–
k_{PF}	–	250 (4.3)	–
k_{RF}	–	$7.3\cdot10^{4}$ (7000)	–
k_{FR}	–	$2.4\cdot10^{5}$ ($1.9\cdot10^{4}$)	
ΔH_n^+ (max)	0.4	0.4	0.1
$I[\mathbf{p}]$	$6.0\cdot10^{-5}$	$6.7\cdot10^{-5}$	$7.1\cdot10^{-5}$

Example equations and initial conditions for Q-cycle 1 are detailed in Appendix 1. Solutions to the equations were repeatedly obtained with systematic variation in the 8 or 9 kinetic parameters, until an integral of errors, related to the differences between the experimental data and the model at 0.1 ms intervals, was minimised. This procedure is known as the Inverse Method [26] and is described in Appendix 2.

Fig. 3 shows a comparison between the predictions of one of the models and the experimental data (deconvoluted from those in Fig. 2) when the kinetic coefficients had been so optimised. These coefficients are shown in Table III, together with the residual error integral. A measure of the sensitivity of the solutions to variations in particular parameters is given by the rate of change of the error integral with respect to that parameter (Δ in Table III).

Discussion

(a) The qualitative meaning of the results

When flash-activated, we assume all P700 is rapidly oxidised. PC reduces $P700^+$ 75% in a short time, after which the remainder of $P700^+$ is reduced in a millisecond time-scale. This slow phase is probably unphysiological (see Ref. 27 for a recent summary). The deconvoluted PC response, which has not previously been clearly observed in thylakoid preparations, is fully consistent with fast oxidation by $P700^+$, followed by reduction by cytochrome *f* combined with continuing slow oxidation by remaining $P700^+$. An estimated 0.9 PC^+ per P700 is available for reduction, just after the flash. The cytochrome *f* signal, of which the oxidation phase is now revealed in clear detail, reflects the balance between fast electron abstraction by PC^+ and slower replacement by quinol. An effect of added ionophore on cytochrome *f* oxidation rate observed by Delosme (Ref. 27, intact cells) would not be expected in our experiments, since the membrane voltage would not have been discharged quickly enough by the 2 μM nonactin used. The chloroplasts were between the 'slow oxidation' state and 'fast-oxidation' state [27], with a $t_{1/2}$ of 200 μs for cytochrome *f* oxidation.

It is quite clear that the speed with which the oxidised high-potential acceptors in the *b/f* complex and PC^+ are reduced depends on the quinol concentration. We continue to observe, with the latest means of deconvoluting for the cytochrome *b*-563 signal, that much less than one haem is reduced, per complex. The electron distribution is assumed to favour PQ^- at the n-sites. Oxidation of cytochrome b-563^- is mostly accounted for by this (but see below).

(b) Quantitative conclusions from the modelling

General: Several hitherto unspecified kinetic coefficients emerge from the modelling. The Inverse Method was adopted as a reasonably objective substitute for repeated, trial and error parameter optimisation (cf. Ref. 15), and also returns a measure of reliability (Δ) for each coefficient.

Using model Q-cycle 1, the optimised value for k_{QL}, was large (10^4–10^5 s^{-1}) compared with k_{QR}, k_{HQ}, k_{QH} (10^2–10^3 s^{-1}), as concluded previously [15] and it was omitted from model Q-cycle 2. Q-cycle models suggested a ratio between k_{HQ} and k_{QH} of 2.4; hence the couples *b*-563(H)/*b*-563(H)$^-$ and PQ$^-$/PQ are separated in reduction potential by $\Delta E_m = 25.3 \ln(k_{HQ}/k_{QH}) = 22$ mV; thus if E_m for *b*(H)/*b*(H)$^-$ is −15 mV [28], that for PQ_n/PQ_n^- is +7 mV.

In the same way, for the couples PC^+/PC and cytochrome *f*/cytochrome *f*$^+$, $\Delta E_m \approx 50$ to 60 mV (PC positive to cytochrome *f*); Joliot and Joliot [4] found a difference of 41 mV under oxidising and single-flash conditions, but concluded that the equilibrium constant was variable, depending on electrostatic interactions between the components. The value 30 mV for a cytochrome *f*-PC adduct was recently found [29].

When the FeS–cytochrome *f* interaction was modelled explicitly, k_{RF} and k_{FR} appeared to be large ($> 10^5$ s^{-1}), but not accurately determined. This indicates a rapid equilibrium, as between the corresponding components in yeast Complex III [30]. The present ratio k_{RF}/k_{FR} suggests that $\Delta E_m \approx -30$ mV (cytochrome *f* negative to R). The parameter α used to express the partition of the electron deficit between R and cytochrome *f* in models Q- and SQ-cycle 1 was 0.73; this gives a ΔE_m of −25 mV. Literature values for E_m for R/R$^+$ [31] and for cytochrome *f*/cytochrome *f*$^+$ [19,29] would suggest a difference of +50 to +60 mV. Our findings may more accurately reflect the in vivo conditions.

The models, except for SQ-cycle 3, predicted a proton uptake per flash from well-spaced turnovers of 0.4 per P700, which is rather less than observed [32], but in conditions where more double turnovers in cytochrome *b*/*f* complexes were expected. It was not possible to distinguish between Q-cycle and SQ-cycle models where the haems were connected. SQ-cycle 3, and any Q-cycle model in which the haems were not internally electronically connected, gave a poor prediction of observed [32] proton uptake and cytochrome *b*-563 reduction; on those grounds, and for the reasons given in (c) below, we believe such models can be neglected.

The data using stigmatellin were also treated by the Inverse Method and models Q-cycle 1 and 2. Parameter optimisation was consistent with a value of k_{QR} of 0.1–0.4 s^{-1} with added inhibitor; stigmatellin was without significant effect on the size of k_{FP}, k_{PF}; poorly estimated rate-coefficients make it difficult to say whether the equilibrium between cytochrome *f* and the Rieske centre was affected.

A parameter representing the dissipation of the one-electron reduced state of the *b*/*f* complex, k_D, was originally introduced into the models because it was thought that the plastoquinone radicals produced

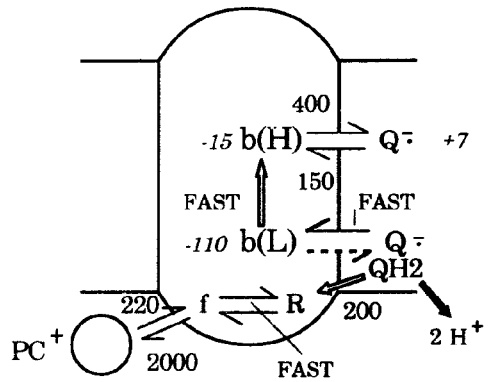

Fig. 5. Schematic of the cytochrome *b*/*f* complex with the median rate-coefficients indicated from the parameter optimisation procedures in the present report. Italicised numbers are reduction potentials in mV, others, reduced rate-coefficients in s^{-1}.

at the n-sites were unbinding with a rate-coefficient of about 5 s^{-1} [32,33] and hence bleeding off the electrons on cytochrome *b*-563(H). The optimised value for this parameter is, however, as high as 100 s^{-1}. We know of no mechanism in the simpler Q-cycle models that would support this rate of dissipation without also reducing the ability to take up protons. If a fixed k_D of 5 s^{-1} was used, the optimisation fit to data for cytochrome *b*$^-$ was poor (Fig. 3a, dashed line), while other components were still adequately predicted.

As seen from Fig. 3, model Q-cycle 2 was able to predict the general form of nearly all the data obtained, especially in times of 0–10 ms. In addition, when [QH2] was varied in the model, rate-coefficients comparable with those in Fig. 4 emerged, giving a further test to the model. A different initial condition with double (to 4) the number of PC per P700, altered only one rate-coefficient in model Q-cycle 1; as expected, k_{PR} was about halved.

The relatively well-determined kinetic coefficients and reduction potentials from this work are summarised in Fig. 5. The kinetic parameters that have been established by the Inverse Method for cytochrome *f* oxidation by PC^+ (for example) cannot generally be compared with literature values because the latter are second order; in thylakoid experiments, absolute concentrations of PC, or of PQH_2, are unknown.

(c) The accuracy of the deconvolution procedure

Several considerations suggest there are no major problems with the deconvolutions. In the reference spectra, there may be contributions to the signals in the 500–600 nm region from the Rieske centre, but they should be small [17]. We used the spectrum of cytochrome *b*-563(H) for deconvolution, and omitted cytochrome *b*-563(L) from several models, since proba-

bly only the high potential form contributes to the observed signal. Reasons for this belief are as follows:

- cytochrome *b*-563(L) did not give any reduction signal in experiments of Nitschke et at. [12]; this cytochrome was either not reduced or the electron was rapidly passed to cytochrome *b*-563(H) and further.
- The relative reduction potentials and separation distance of the high and low potential cytochrome *b*-563's suggest theoretically a very fast transfer, in fact a kinetic coefficient of about 10^5 s^{-1} [15].
- There is evidence of direct electron transfer between the corresponding haems in the mitochondrial cytochrome b/c_1 complex [34].

The electrochromic contribution was taken as a linear function of membrane p.d. at each measuring wavelength. This is more likely to be an acceptable approach for small p.d. values, whereas it was not for PS bacteria, where $\Delta\Psi$ of several hundred millivolts were considered [35], and quadratic coefficients were necessary.

Are there other chloroplast components yielding signals of significance? We tested for cytochrome *b*-559 and found no significant flash-induced signal whatever in the deconvolution; further, whether we used a 4×4 matrix or 5×5 matrix did not significantly affect the shape of the cytochrome *f* and *b*-563 signals. That no kinetic signal originating from the cytochrome *b/f* complex is found for cytochrome *b*-559 is not necessarily surprising; a signal seldom appears for PS-II-related cytochrome *b*-559 during the turnover of that system in physiological conditions.

(d) Control of a Q- or SQ-cycle

Volz and Rumberg [36] have suggested that the second electron from PQH_2 oxidation may be transferrable to R^+ under some conditions; the electron path through the *b*-563 cytochromes not being initiated, the cycle that would lead to proton uptake near n-sites is prevented. It was suggested that the process of 'linear' electron transfer of both electrons from PQH_2 would be favoured when cytochrome *f* was in an oxidised state. Such a process has been inferred from experiments with subchloroplast particles [11]. Rich [37], however, has argued that protonmotive Q-cycle operation of the cytochrome *b/f* complex is the norm. Further experiments are underway to test the idea in chloroplasts.

Acknowledgments

The project was supported by the Australian Research Council and Flinders University. We thank Western Mining Corporation for the loan of a YAG laser, Dr. Jim Richards, Optical Physics Group, Defence Science and Technology Organisation, Salisbury, South Australia, for increasing its frequency-doubled output and devising the Raman-shifting modification, and West Hiscock for essential help in laser operation and maintenance. Purified plastocyanin and cytochrome *b/f* complexes were kindly made available by, or prepared with the collaboration of Prof. G. Hauska (University of Regensburg, Germany) during a visit by A.B.H., which is gratefully acknowledged. Stigmatellin was generously provided by Prof. Dr. G. Höfle. Ian Modistach and Bruce White are thanked for electronic developments, Sue Tyerman for a software program.

References

1 Joliot, P. and Joliot, A. (1988) Biochim. Biophys. Acta 933, 319–333.
2 Rich, P.R. and Bendall, D.S. (1980) Biochim. Biophys. Acta 591, 153–161.
3 Joliot, P. and Joliot, A. (1984a) Biochim. Biophys. Acta 765, 210–218.
4 Joliot, P. and Joliot, A. (1984b) Biochim. Biophys. Acta 765, 219–226.
5 Houchins, J.P. and Hind, G. (1983) Biochim. Biophys. Acta 725, 138–145.
6 Selak, M.A. and Whitmarsh, J. (1982) FEBS Lett. 150, 286–92.
7 Jones, R.W. and Whitmarsh, J. (1985) Photobiochem. Photobiophys. 9, 119–27.
8 Jones, R.W. and Whitmarsh, J. (1988) Biochim. Biophys. Acta 933, 258–268.
9 Moss, D.A. and Rich, P.R. (1987) Biochim. Biophys. Acta 894, 189–197.
10 Rich, P.R., Heathcote, P. and Moss, D.A. (1987) Biochim. Biophys. Acta 892, 138–151.
11 De Wolf, F.A., Krab, K., Visschers, R.W., De Waard, J.H. and Kraayenhof, R. (1988) Biochim. Biophys. Acta 936, 487–503.
12 Nitschke, W., Hauska, G. and Crofts, A.R. (1988) FEBS Lett. 232, 204–208.
13 Nitschke, W., Hauska, G. and Rutherford, A.W. (1989) Biochim. Biophys. Acta 974, 223–226.
14 Hope, A.B., Liggins, J. and Matthews, D.B. (1988) Aust. J. Plant Physiol. 15, 695–703.
15 Hope, A.B., Liggins, J. and Matthews, D.B. (1989) Aust. J. Plant Physiol. 16, 353–364.
16 Rieske, J.S., MacLennan, D.H. and Coleman, R. (1964) Biochem. Biophys. Res. Commun. 15, 338–344.
17 Bouges-Bocquet, B. (1980) FEBS Lett. 117, 54–55.
18 Hauska, G., Herold, E., Huber, C., Nitschke, W. and Sofrova, D. (1989) Z. Naturforsch. 44c, 462–467.
19 Emrich, H.M., Junge, W. and Witt, H.T. (1969) Z. Naturforsch. 24b, 1144–1146.
20 Dolan, E. and Hind, G. (1974) Biochim. Biophys. Acta 357, 380–385.
21 Rich, P.R., Madgwick, S.A. and Moss, D.A. (1991) Biochim. Biophys. Acta 1058, 313–328.
22 Mitchell, P. (1976) J. Theor. Biol. 62, 327–367.
23 Wikström, M. and Krab, K. (1986) J. Bioenerg. Biomembr. 18, 181–193.
24 Hope, A.B. and Matthews, D.B. (1988) Aust. J. Plant Physiol. 15, 567–583.
25 Furbacher, P.N., Girvin, M.E. and Cramer, W.A. (1989) Biochemistry 28, 8990–8998.
26 Novak, U. and Deuflhard, P. (1983) in Progress in Scientific Computation, Vol. 2: Numerical Treatment of Inverse Problems

in Differential and Integral Equations. (Deuflhard, P. and Hairer, E., eds.), pp.13–26, Birkhäuser, Boston.
27 Delosme, R. (1991) Photosyn. Res. 29, 45–54.
28 Kramer, D.M. and Crofts, A.R. (1990) in 'Current Research in Photosynthesis' (Baltscheffsky, M., ed.), Vol. III, pp. 283–286, Kluwer, Dordrecht.
29 Morand, L.Z., Frame, M., Krogmann, D.W. and Davis, D.J. (1990) in Current Research in Photosynthesis (Baltscheffsky, M., ed.), Vol. III, pp. 303–306, Kluwer, Dordrecht).
30 T'sai, A-L, Olsen, J.S. and Palmer, G. (1983) J. Biol. Chem. 258, 2122–2125.
31 Trumpower, B. (1981) Biochim. Biophys. Acta 639, 129–155.
32 Hope, A.B. and Rich, P.R. (1989) Biochim. Biophys. Acta 975, 96–103.
33 Pace, R.J., Hope, A.B. and Smith, P. (1991) Biochim. Biophys. Acta, in press.
34 West, I.C., Mitchell, P. and Rich, P.R. (1988) Biochim. Biophys. Acta 933, 35–41.
35 Venturoli, G., Virgili, M., Melandri, B.A. and Crofts, A.R. (1987) FEBS Lett. 219, 477–484.
36 Volz, E. and Rumberg, B. (1990) in Current Research in Photosynthesis (Baltscheffsky, M., ed.), Vol. III, pp. 275–278, Kluwer, Dordrecht.
37 Rich, P.R. (1988) Biochim. Biophys. Acta 932, 33–42.
38 Chow, W.S. and Anderson, J.M. (1987) Aust. J Plant Physiol. 14, 9–19.

Appendix 1

Model Q-cycle 1: solving for the variables

1. The reactions
(similar to those in Ref. 15):

$$PC^{+} + RH \underset{k_{PR}}{\overset{k_{RP}}{\rightleftharpoons}} PC + R^{\cdot} H$$

$$PQH_2 + R^{\cdot} H \xrightarrow{k_{QR}} Rp^{\cdot} H \xrightarrow{k_{QL}} RH \quad n + 2H_p^{+}$$

$$RH \quad n \underset{k_{OH}}{\overset{k_{HO}}{\rightleftharpoons}} RHn \xrightarrow{k_D} RH + PQ$$

$$PC^{+} + Rp^{\cdot} H \underset{k_{PR}}{\overset{k_{RP}}{\rightleftharpoons}} PC + R^{\cdot} p^{\cdot} H$$

$$R^{\cdot} p^{\cdot} H \xrightarrow{k_{QL}} R^{\cdot} H \quad n + 2H_p^{+}$$

$$R^{\cdot} H \quad n \underset{k_{OH}}{\overset{k_{HO}}{\rightleftharpoons}} R^{\cdot} Hn \xrightarrow{k_D} R^{\cdot} H + PQ$$

$$PC^{+} + RH \quad n \underset{k_{PR}}{\overset{k_{RP}}{\rightleftharpoons}} PC + R^{\cdot} H \quad n$$

$$PQH_2 + R^{\cdot} H \quad n \xrightarrow{k_{QR}} Rp^{\cdot} H \quad n$$

$$\xrightarrow{k_{QL}} RL \quad H \quad n + 2H_p^{+}$$

$$RL \quad H \quad n \xrightarrow{k_{HO}} RH + PQH_2 - 2H_n^{+}$$

$$Rp^{\cdot} H \quad n \underset{k_{OH}}{\overset{k_{HO}}{\rightleftharpoons}} Rp^{\cdot} Hn \xrightarrow{k_D} Rp^{\cdot} H + PQ$$

$$PC^{+} + RHn \underset{k_{PR}}{\overset{k_{RP}}{\rightleftharpoons}} PC + R^{\cdot} Hn$$

$$PQH_2 + R^{\cdot} Hn \xrightarrow{k_{QR}} Rp^{\cdot} Hn$$

$$\xrightarrow{k_{QL}} RH + 2H_p^{+} + PQH_2 - 2H_n^{+}$$

A form of the cytochrome *b/f* complex such as represented by, for example, $Rp^{+}\ H^{-}n$ has the following meaning: the complex has its Rieske centre reduced and its cytochrome *b*-563(H) reduced; it has PQH_2^{+} bound at the p-site and PQ bound at the n-site. The "H" in such forms should not be confused with "H_p^{+}", a hydrogen ion.

2. The differential equations

$$\dot{y}_1 = -k_{RP} y_1 (y_2 + y_5 + y_6 + y_8) + k_{PR}(2 - y_1)(y_3 + y_9 + y_{10} + y_{11})$$

$$\dot{y}_2 = -k_{RP} y_1 y_2 + k_{PR}(2 - y_1) y_3 + k_D y_8 + k_{HO} y_{13} + k_{QL} y_{15}$$

$$\dot{y}_3 = k_{RP} y_1 y_2 - k_{PR}(2 - y_1) y_3 - k_{QR} y_3 y_4 + k_D y_{11}$$

$$\dot{y}_4 = -k_{QR} y_4 (y_3 + y_{10} + y_{11}) + k_{HO} y_{13} + k_{QL} y_{15}$$

$$\dot{y}_5 = k_{QR} y_3 y_4 - k_{QL} y_5 - k_{RP} y_1 y_5 + k_{PR}(2 - y_1) y_9 + k_D y_{15}$$

$$\dot{y}_6 = k_{QL} y_5 - k_{HO} y_6 + k_{OH} y_8 - k_{RP} y_1 y_6 + k_{PR}(2 - y_1) y_{10}$$

$$\dot{y}_7 = k_{QL} (y_5 + y_9 + y_{12} + y_{15})$$

$$\dot{y}_8 = k_{HO} y_6 - y_8 (k_{OH} + k_D) - k_{RP} y_1 y_8 + k_{PR}(2 - y_1) y_{11}$$

$$\dot{y}_9 = k_{RP} y_1 y_5 - k_{PR}(2 - y_1) y_9 - k_{QL} y_9$$

$$\dot{y}_{10} = k_{QL} y_9 + k_{OH} y_{11} - k_{HO} y_{10} + k_{RP} y_1 y_6$$

$$- k_{PR}(2 - y_1) y_{10} - k_{QR} y_4 y_{10}$$

$$\dot{y}_{11} = k_{HO} y_{10} - y_{11} (k_{OH} + k_D) - k_{QR} y_4 y_{11} + k_{RP} y_1 y_8$$

$$- k_{PR}(2 - y_1) y_{11}$$

$$\dot{y}_{12} = k_{QR} y_4 y_{10} - y_{12} (k_{QL} + k_{HO}) + k_{OH} y_{15}$$

$$\dot{y}_{13} = k_{QL} y_{12} - k_{HO} y_{13}$$

$$\dot{y}_{14} = k_{HO} y_{13} + k_{QL} y_{15}$$

$$\dot{y}_{15} = k_{HO} y_{12} - y_{15} (k_{OH} + k_{QL} + k_D) + k_{QR} y_4 y_{11}$$

Notes:
1 The total PC is taken as 2 per P700; hence $[PC] = 2 - [PC^{+}]$.
2 $[\text{cyt } b\text{-}563^{-}] = y_6 + y_{10} + y_{12} + 2y_{13}$.
3 Other observables such as ΔH_p^{+} from the table below.

3. Equation variables and initial values (per P700) just after a flash

Variable number	Form	initial value
y_1	$[PC^+]$	0.9
y_2	[RH]	$[b/f]/[P700]$ [a]
y_3	$[R^-H]$	0.0
y_4	$[PQH_2]$	6.0 [b]
y_5	$[Rp^+H]$	0.0
y_6	$[RH^-n]$	0.0
y_7	ΔH_p^+	0.0
y_8	$[RHn^-]$	0.0
y_9	$[R^-p^+H]$	0.0
y_{10}	$[R^-H^-n]$	0.0
y_{11}	$[R^-Hn^-]$	0.0
y_{12}	$[Rp^+H^-n]$	0.0
y_{13}	$[RL^-H^-n]$	0.0
y_{14}	ΔH_n^+	0.0
y_{15}	$[Rp^+Hn^-]$	0.0

[a] This equals 1.0 in our chloroplasts, grown in moderate (200–400 μmol $h\nu$ m^{-2} s^{-1}) illuminance [38].
[b] PQ pool fully reduced.

Appendix 2

The Inverse Method

The inverse method is a technique developed to find the optimal rate coefficients in kinetic equations from given experimental data. Two basic approaches, called the discrete and the continuous functional, are described by Nowak and Deuflhard [26]. We summarise the continuous functional approach here.

Consider a system of chemical reactions which can be modelled by a system of n nonlinear, ordinary differential equations depending on q parameters, $p_1, \ldots, p_q$, viz.,

$$\dot{y}_i = f_i(y_j; p_s), \quad i,j = 1,\ldots,n; \quad s = 1,\ldots,q. \tag{A2.1}$$

given a set of initial conditions $y_i(0)$, $i = 1,\ldots,n$. Let us denote the solution of (A2.1), using the bold notation, as the vector $\mathbf{y}(t, \mathbf{p})$.

The idea behind the inverse method is to find the best possible set of parameters so that the solution fits the experimental data measured over m time intervals $t_1, \ldots, t_m$. Here two problems are likely to arise:

(i) As noted in Appendix 1, in connection with [cytochrome b-563$^-$], one may be confined to measuring combinations of the variables y_i, instead of of the individual variables $y_1, \ldots, y_n$.

(ii) The second one may arise if all the variables cannot be measured.

The solution to the problem (i) is obtained by creating a new set of variables $\hat{y}_1, \ldots, \hat{y}_n$ in terms of the old $y_1, \ldots, y_n$ so that each of the new variables may be individually measured. After rewriting the equations in terms of $\hat{y}_1, \ldots, \hat{y}_n$, the hats, $\hat{}$, are dropped so that the modified equations will acquire the form (A2.1).

To explain the solution to the problem (ii), let us consider the *ideal* situation where all of the variables (modified as above, if necessary) can be measured. Let the experimental values be

$$(t_1, z_i(t_1)), \ldots, (t_m, z_i(t_m)), \quad i = 1,\ldots,n, \tag{A2.2}$$

that is, we have an $m \times n$ data points so that the (new) variables y_i in the model correspond to the measured variables z_i.

Turning to the more realistic situation, let us suppose one variable, say y_3,is not observable. In this case, we put the experimentally unknown values of y_3 at $t = t_b$ equal to the computed values of y_3 at $t = t_b$, $b = 1,\ldots,m$. These *computed* values of y_3 at $t = t_b$ are then assumed to be the *measured* values z_3 at $t = t_b$. Hence, using such a procedure for as many of the non-observable variables as necessary and adding to this set the set of all measurements, we obtain a complete list of values for all the quantities in (A2.2).

Let us now return to the equations (A2.1) and differentiate them with respect to each of the parameters. Noting that the time variable and the parameters are independent, we get

$$\frac{\dot{\partial y_i}}{\partial p_r} = \sum_{h=1}^{n} \frac{\partial f_i}{\partial y_h} \frac{\partial y_h}{\partial p_r} + \frac{\partial f_i}{\partial p_r},$$

$$i = 1,\ldots,n, \quad r = 1,\ldots,q, \tag{A2.3}$$

with the initial conditions

$$\frac{\partial y_i}{\partial p_r}(0) = 0. \tag{A2.4}$$

Let us summarise (A2.1) and (A2.3) with the relevant initial conditions as

$$\begin{aligned} &\dot{\mathbf{y}} = \mathbf{f}(\mathbf{y}, \mathbf{p}), \\ &\dot{\mathbf{y}}_\mathbf{p} = \mathbf{f}_\mathbf{y}\mathbf{y}_\mathbf{p} + \mathbf{f}_\mathbf{p}, \\ &\mathbf{y}(0) = \text{given}, \\ &\mathbf{y}_\mathbf{p}(0) = \mathbf{0}. \end{aligned} \tag{A2.5}$$

Note that $\mathbf{y}_\mathbf{p}$ is an $n \times q$ matrix.

Now, corresponding to (A2.5) are the equations using the experimental data, viz.,

$$\begin{aligned} &\dot{\mathbf{z}} = \mathbf{f}(\mathbf{z}, \mathbf{p}), \\ &\dot{\mathbf{z}}_\mathbf{p} = \mathbf{f}_\mathbf{z}\mathbf{z}_\mathbf{p} + \mathbf{f}_\mathbf{p}. \end{aligned} \tag{A2.6}$$

with the initial conditions

$$\begin{aligned} &\mathbf{z}(0) = \mathbf{y}(0), \\ &\mathbf{z}(t_h) = \text{measured (cf. (A2.2))}, \quad h = 1, \ldots, m, \\ &\mathbf{z}_{\mathbf{p}}(0) = 0, \\ &\mathbf{z}_{\mathbf{p}}(t_h) = 0, \quad h = 1, \ldots, m. \end{aligned} \tag{A2.7}$$

What is being in done in (A2.5) is to integrate the model equations using the given initial conditions over the time interval $0 \le t \le t_m + \Delta t$, with Δt being a typical step size, whereas in (A2.6)–(A2.7), we integrate the same set of equations, using the experimental values at $t = 0$ and at $t = t_h$ as initial values for the intervals $[0, t_1]$ and $[t_h, t_{h+1}]$, respectively.

Next, let the error vector be denoted by

$$\mathbf{e}(t) = \mathbf{y}(t, \mathbf{p}) - \mathbf{z}(t, \mathbf{p}). \tag{A2.8}$$

The inverse method is based on finding the parameter vector $\mathbf{p}$ so as to minimise the scalar-valued integral

$$I[\mathbf{p}] = \sum_{h=1}^{m} \int_0^{t_h} \mathbf{e}(t)^T \mathbf{D}(t) \mathbf{e}(t)\, dt, \tag{A2.9}$$

where $\mathbf{D}(t)$ is a positive-definite weighting matrix and the superscript T denotes the transpose. Symbolically, we represent an integral of the form (A2.9) through

$$I[\mathbf{p}] = \langle \mathbf{e}, \mathbf{e} \rangle. \tag{A2.10}$$

In the present work, we have assumed that the matrix $\mathbf{D}$ is the identity matrix in (A2.9) and elsewhere.

In order to minimise the error $I[\mathbf{p}]$, one needs to integrate the equations (A2.1) for various parameters and find the minimum. Difficulties arise in deciding which of the parameters need to be changed and what the respective increments ought to be; the inverse method can answer these questions. We shall now describe the next step in using this technique.

In the ideal situation, the model answers and the experimental values would agree at $t = 0$ and at each $t = t_h$ and the integral $I[\mathbf{p}]$ would be zero. Because this is unlikely to occur, we now find the parametric derivative of the error $\mathbf{e}$, i.e.,

$$\mathbf{e}_{\mathbf{p}}(t) = \mathbf{y}_{\mathbf{p}}(t) - \mathbf{z}_{\mathbf{p}}(t). \tag{A2.11}$$

Note that the matrices $\mathbf{y}_{\mathbf{p}}$ and $\mathbf{z}_{\mathbf{p}}$ are available through the solutions of (A2.5)–(A2.7) and hence $\mathbf{e}_{\mathbf{p}}(t)$ is an $n \times q$ matrix.

Let us now define two new integrals using the notation (A2.10). The first one is

$$\mathbf{I}'[\mathbf{p}] = \langle \mathbf{e}_{\mathbf{p}}, \mathbf{e} \rangle, \tag{A2.12}$$

and this is a q-vector. The next one is

$$\mathbf{I}''[\mathbf{p}] = \langle \mathbf{e}_{\mathbf{p}}, \mathbf{e}_{\mathbf{p}} \rangle, \tag{A2.13}$$

and this is a $q \times q$ matrix. Now, the ordinary Gauss-Newton iterative method tells us that in order to find the kth increment $\Delta \mathbf{p}^k$ so that we are following the steepest descent in going from $I[\mathbf{p}^k]$ to $I[\mathbf{p}^k + \Delta \mathbf{p}^k]$, we must find the increment through

$$\mathbf{I}''[\mathbf{p}^k] \Delta \mathbf{p}^k = -\mathbf{I}'[\mathbf{p}^k]. \tag{A2.14}$$

In numerical work, it is found that the matrix $\mathbf{I}''$ is not always positive definite and hence the increment can only be calculated approximately.

Returning to the problem at hand, we calculate $I[\mathbf{p}]$ for an educated guess of the initial vector $\mathbf{p}^0$. Then we find the next value through

$$\mathbf{p}^{k+1} = \mathbf{p}^k + \lambda_k \Delta \mathbf{p}^k, \tag{A2.15}$$

where λ_k are scalars to be found in the set $[1, 1/2, \ldots, 1/64]$. The scalar is chosen at each iteration so that

$$I[\mathbf{p}^k + \lambda_k \Delta \mathbf{p}^k] \le I[\mathbf{p}^k] + \tfrac{1}{2} \lambda_k \mathbf{I}'[\mathbf{p}^k]^T \Delta \mathbf{p}^k. \tag{A2.16}$$

This last procedure is described as the damping strategy by Nowak and Deuflhard [26].

If, after finding a $\Delta \mathbf{p}^k$ through (A2.14), such a λ_k cannot be found, then we are near a local minimum for $I[\mathbf{p}]$. To judge whether we are near a global minimum, it is necessary to vary the initial guess of $\mathbf{p}^0$ and repeat the calculations.

In this paper, we have provided the absolute values of the integral $I[\mathbf{p}]$ in Table III and because the errors are very small, we have assumed that we are near a global minimum. Also, the parameters $p_1, \ldots, p_q$ become k_{RP}, k_{PR}, etc., which are the rate constants of the relevant reaction equations. The final values of the $\Delta \mathbf{p}^k$ values are referenced as (Δ). If the number (Δ) is positive (resp. negative), then the corresponding parameter is increasing (resp. decreasing) as the minimum is approached. Thus each (Δ) provides a loose measure of the likely error in the individual reduced rate coefficients. It must be emphasised that this measure of the error should be viewed as a percentage of the relevant parameter value rather than as an item by itself.